Published in final edited form as:
Biomaterials. 2010 September ; 31(27): 7132–7138. doi:10.1016/j.biomaterials.2010.06.008.

Noninvasive visualization of *in vivo* release and intratumoral distribution of surrogate MR contrast agent using the dual MR contrast technique

Yoshinori Onuki[1,#], **Igor Jacobs**[2], **Dmitri Artemov**[1], and **Yoshinori Kato**[1,*]

[1]JHU ICMIC Program, The Russell H. Morgan Department of Radiology and Radiological Science, Johns Hopkins University School of Medicine, Baltimore, Maryland, U.S.A. [2]Department of Biomedical Engineering, Eindhoven University of Technology, Eindhoven, The Netherlands

Abstract

A direct evaluation of the *in vivo* release profile of drugs from carriers is a clinical demand in drug delivery systems, because drug release characterized *in vitro* correlates poorly with *in vivo* release. The purpose of this study is to demonstrate the *in vivo* applicability of the dual MR contrast technique as a useful tool for noninvasive monitoring of the stability and the release profile of drug carriers, by visualizing *in vivo* release of the encapsulated surrogate MR contrast agent from carriers and its subsequent intratumoral distribution profile. The important aspect of this technique is that it incorporates both positive and negative contrast agents within a single carrier. GdDTPA, superparamagnetic iron oxide nanoparticles, and 5-fluorouracil were encapsulated in nano- and microspheres composed of poly(D,L-lactide-*co*-glycolide), and which was used for a model carrier. *In vivo* studies were performed with orthotopic xenograft of human breast cancer. The MR-based technique demonstrated here has enabled visualization of the delivery of carriers, and release and intratumoral distribution of the encapsulated positive contrast agent. This study demonstrated proof-of-principle results for the noninvasive monitoring of *in vivo* release and distribution profiles of MR contrast agents, and thus, this technique will make a great contribution to the field.

Keywords

MRI (magnetic resonance imaging); Molecular imaging; Drug release; *In vivo* test; Nanoparticle

*Corresponding author: Yoshinori Kato, Ph.D., Phone: +1-443-287-4426, FAX: +1-410-614-1948, ykato@mri.jhu.edu. Address: Johns Hopkins University School of Medicine, Dept. of Radiology, 720 Rutland Ave., Traylor Bldg. #217, Baltimore, MD 21205, U.S.A.
#Current address: Department of Pharmaceutics, Hoshi University, 2-4-41 Shinagawa-ku, Tokyo 142-8501, Japan

Appendix. Supplementary material
Supplementary data associated with this article can be found, in online version.

1. Introduction

Now, in the 21st century, attention is particularly focused on the clinical application of biomaterials in biomedical field, which includes biodegradable drug/gene carriers, implanted devices, and tissue engineering. Intrinsic properties of biomaterials used for the controlled release formulations, such as nano- or micro-sized drug carriers or implanted devices, play a crucial role in an optimal treatment regimen. Although it is known that a number of factors contribute to drug release, such as materials, size, and surface charge of carriers, as well as the molecular size, hydrophilicity, and net charge of the drug molecules, further investigations regarding drug release *in vivo* are in great demand. Current strategies to monitor the *in vivo* release profile of drugs include indirect measurements of drug concentrations in blood and urine samples or invasive measurements of biopsy tissues, and, to date, only limited studies of noninvasive *in vivo* release monitoring have been reported [1,2]. Radionuclide imaging is not optimal for this purpose due to the innately short half-life of radioisotopes, and also because discrimination between encapsulated and released markers, as yet, is not possible. Activated optical imaging probes have been developed [3,4], but, these agents have, as yet, limited applications in clinical settings due to low spatial resolution and depth penetration limits. To this end, a noninvasive MR-based multiparametric imaging technique has been developed to monitor the release of drug molecules either directly by MR spectroscopy or indirectly by MRI with gadolinium-based contrast agents [5]. Conventional contrast-enhanced MRI techniques that use a single contrast agent cannot distinguish between encapsulated and released molecules. The key advantage of the newly developed technique is that it can demarcate released cargo molecules from encapsulated molecules (Fig. 1). The principle of this technique is that the positive-enhancement T_1 effects of encapsulated GdDTPA are cancelled out by loading the carrier or device with superparamagnetic iron oxide (SPIO) nanoparticles, whereas the T_1 effect of GdDTPA released from the carrier/device becomes apparent once GdDTPA molecules diffuse beyond the range of the T_2/T_2* effects of SPIO. Similarly, encapsulated drug molecules that are co-encapsulated with SPIO have broad resonance lines in MRS due to the T_2* effect of SPIO particles [6], while the released drug molecules give a narrow resonance line once drug molecules diffuse beyond the range of the T_2* effects of SPIO. Initially, the concept behind this strategy was validated using an *in vitro* model system [5]. Due to their large molecular size, SPIO nanoparticles have a much shorter diffusion range compared to the small molecular contrast agent, GdDTPA. For instance, the intratumoral distribution of larger molecules is restricted due to the short diffusion distance from the vascular surface, compared to smaller molecules [7], which supports the feasibility of this technique *in vivo*, in this case in solid tumors. In this study, to demonstrate the potential use of this new MRI technique for noninvasive release monitoring *in vivo*, the release of a surrogate MR contrast agent, GdDTPA, from poly(D,L-lactide-*co*-glycolide) (PLGA) nano/microspheres was monitored in mice bearing orthotopic MCF-7 breast tumor xenograft.

2. Materials and methods

2.1. Chemicals, animals, and cell lines

Omniscan® (GdDTPA-BMA, 0.5 M) was purchased from GE Healthcare (Chalfont St. Giles, Buckinghamshire, U.K.). Feridex® (SPIO, 11.2 mg/mL) was purchased from Bayer Healthcare Pharmaceuticals, AG (Leverkusen, Germany). Fluorouracil injection (5-FU, 50 mg/mL) was obtained from APP Pharmaceuticals, Inc. (Schaumburg, IL, USA). Poly(D,L-lactide*co*-glycolide) (PLGA, M.W. = 40–75 kDa), Span 80, poly(vinylalcohol) (PVA, M.W. = 8–10 kDa), and poly(ethylene glycol)-*block*-poly(propylene glycol)-*block*-poly(ethylene glycol) copolymer (PEG-PPG-PEG, average Mn: 8.4 kDa) were purchased from Sigma-Aldrich Co. (St. Louis, MO, U.S.A.). Mouse plasma was obtained from Innovative Research (Novi, MI, U.S.A.). Nitric acid (*Trace*SELECT®) was obtained from Fluka (St. Louis, MO,

U.S.A.). Water and methanol for the HPLC used were of HPLC grade. All of the other chemicals used were of analytical grade.

Severe combined immunodeficient (SCID) mice (female, 4–6 weeks old, 19–23 g) were purchased from NCI (Bethesda, MD, U.S.A.). Approval from the institutional animal care and use committee preceded all animal experiments in the present study. The culture of MCF-7 estrogen-dependent human breast carcinoma cells and the orthotopic inoculation of the cells into the mammary fat pad of a mouse were performed according to the previous study [8]. At least three animals were used for each *in vivo* study.

2.2. Preparation of contrast agent-loaded PLGA nano/microspheres

PLGA nano/microspheres (NS-GdDTPA/SPIO/5-FU and MS-GdDTPA/SPIO/5-FU, respectively) incorporating 5-FU, GdDTPA, and SPIO were prepared using a double-emulsion solvent evaporation method. Briefly, a mixture of Omniscan® (250 μL), a standard 5-FU solution (50 mg/mL, 250 μL) and Feridex® (50 μL) was added dropwise to 5 mL of dichloromethane containing 50 mg of PLGA and 20 mg of Span 80 as an emulsifier, to prepare NS-GdDTPA/SPIO/5-FU. For the preparation of MS-GdDTPA/SPIO/5-FU, 1 mL of dichloromethane containing 250 mg of PLGA, was used instead. The mixture was sonicated for 10 min on ice, which resulted in the formulation of a water-in-oil (w/o) emulsion. The w/o emulsion was poured onto the outer aqueous layer (PBS containing 1% PVA, 0.2% PEP-PPG-PEG, 1% NaCl), and sonicated again for 3 min on ice to obtain a water-in-oil-in-water (w/o/w) emulsion. To obtain nano- and micro-sized spheres, 7.5 and 5.0 mL of the outer aqueous phase were used, respectively (see Supplemental material, Fig. S1). After the evaporation for 1 hr at 37 °C to remove dichloromethane, NS-GdDTPA/SPIO/5-FU and MS-GdDTPA/SPIO/5-FU were washed with purified water several times by centrifugation (3 min, 4 °C) at 8,000 ×*g* and at 360 ×*g*, respectively, lyophilized, and stored in the refrigerator until use.

2.3. Characterization of PLGA nano/microspheres

To determine particle size, size distribution, and ζ-potential of the resultant PLGA nano/microspheres, dynamic laser-light scattering (DLS) measurements were performed using a Zetasizer Nano-ZS90 (Malvern Instruments Ltd., Worcestershire, UK) with a He-Ne laser system, which is operated at 633 nm and 25 ±1 °C, and the scattered light is measured at an angle of 90°. The morphology of PLGA nano/microspheres was characterized with a scanning electron microscope (SEM) (LEO1550, Carl Zeiss, Inc., Thornwood, NY, U.S.A.). For sample preparation, lyophilized PLGA nano/microspheres were dispersed in purified water (0.05 mg/mL), and the droplets were dried on the surface of a cover glass at room temperature. They were coated with gold sputter from the vapor on an auto fine coater.

Loading amounts of 5-FU and GdDTPA were determined by UV detection with reverse phase high-performance liquid chromatography (HPLC), and by T_1 relaxation time measurements with MRI, respectively, after destruction of PLGA nano/microspheres with dichloromethane. The quantification analysis with HPLC for 5-FU was performed as in Coe *et al.* [9], with minor modifications. Briefly, 1 mg of lyophilized nano/microspheres was dissolved in 300 μL of dichloromethane, and then 150 μL of purified water was added to the sample to extract 5-FU. After vortexing, 20 μL of the sample solution was directly injected into a Waters 1525 binary HPLC pump equipped with a Waters Symmetry® C18 reversed phase column (4.6 mmφ × 150 mm) and a Waters Ultrahydrogel Guard Column (6.0 mmφ × 40 mm). A Waters 2487 dual λ absorbance detector was set at 266 nm. Potassium phosphate (10 mM, pH 5.5) and methanol were used as the mobile phase A and B, respectively, and the elution program was as follows: run mobile phase A for first 5 min, increase mobile phase B from 0% to 25% over next 1 min, and maintain mobile phase B at 25% for 3 min. The initial

conditions were restored by decreasing mobile phase B to 0% over 1 min, and the column was equilibrated with 100% mobile phase A for 10 min. The flow rate was 0.8 mL/min, and HPLC analysis was performed at room temperature. The Breeze 3.30 program (Waters Corp., Milford, MA, USA) was used as acquisition and analysis software.

The quantification analysis with MRI for GdDTPA was performed in the same manner as in our previous report [5]. The T_1 relaxation time of the sample solution was measured on a Bruker 9.4T horizontal bore spectrometer (Bruker Biospin GmbH, Rheinstetten, Germany). The quantification of GdDTPA was also conducted with inductively-coupled plasma mass spectrometry (ICP-MS, ParkinElmer, Waltham, MA, U.S.A.). For the extraction of GdDTPA for ICP-MS measurement, 2% (v/v) nitric acid (*Trace*SELECT®) was used as an extraction medium, rather than purified water. The T_1 relaxation time measurement was consistent with the results obtained by the ICP-MS measurement.

2.4. In vitro release characteristics

PLGA nano/microspheres (40 mg) were dispersed into 2 mL of 10% (v/v) mouse plasma in PBS. Each suspension was incubated with gentle shaking at 37 °C throughout the experiment. At designated intervals, an aliquot (500 μL) was withdrawn and the supernatant was separated from the PLGA nano/microspheres by centrifugation at 8,000 ×*g* for 3 min at 4 °C. After collecting the supernatant, the pellet of nano/microspheres was resuspended in the same volume of fresh release medium (500 μL), and then returned to the sample suspension. The amounts of 5-FU and GdDTPA in the supernatant were determined with HPLC and MRI, respectively, as described above.

2.5. Visualization of in vivo release of GdDTPA from PLGA nanospheres

MRI was carried out on a Bruker horizontal bore 9.4T spectrometer equipped with shielded gradients. The Paravision 3.0.2 program (Bruker Biospin, GmbH) was used as acquisition software. *In vivo* studies were performed with an orthotopic human breast carcinoma MCF-7 grown in female SCID mice. Each anesthetized mouse was immobilized in the probe, and the tumor was positioned in the $^{1}H/^{19}F$ RF coil. The tail vein of the mouse was catheterized before placing the animal in the magnet. During MRI experiments, animals were maintained under gas anesthesia (1% isoflurane in a mixture of 70% O_2 and 30% N_2 at 1 L/min), and animal body temperature was maintained at 37 °C by a circulating water thermo-pad, and respiration rate was monitored with a Bruker dedicated physiology monitoring system, using a pressure pad and a pressure transducer. After tuning the probe and shimming the magnet, tri-planar scout images were acquired to determine the position of the imaging slices. MRI was acquired before, 30 min, and 2.5 hr after administration of NS-GdDTPA/SPIO/5-FU. Mice received an intravenous administration of 200 μL of NS-GdDTPA/SPIO/5-FU suspension at a dose of 40 mg per mouse, which is equivalent to 25 and 8 μmol/kg of GdDTPA and 5-FU, respectively. To obtain both released GdDTPA and SPIO distribution images, a 3D fast spin echo (RARE: Rapid Acquisition with Relaxation Enhancement) sequence with an effective echo time (TE) of 50 ms and a repetition time (TR) of 1,000 ms was acquired. This technique provides fast acquisition of 3D volumes with a uniform spatial resolution of up to 100 μm *in vivo* within 30 min experimental time. For the quantitative T_1 map, a 3D RARE pulse sequence with a TE of 50 ms, and five different TRs (250, 500, 1,000, 2,000, and 4,000 ms) was acquired with a spatial resolution of 0.125×0.125μ0.0625 mm (128×80×40 matrix zero-filled to 128×128×128, field of view = 16×16×8 mm). Quantification of T_1 was carried out in the same manner as in the *in vitro* study. For T_2* acquisition, a 3D fast low-angle shot (FLASH) pulse sequence was used with the following parameters: TE/TR = 7/100 ms; number of acquisitions = 2; and flip angle ≈32°. Final analysis was performed with the ImageJ® program (National Institutes of Health). T_1 maps were reconstructed with in-house software written in the IDL programming environment

(ITT Visual Information Solutions, Boulder, CO, U.S.A.), and 3D images were visualized with the Amira graphic package (TGS Inc., San Diego, CA, U.S.A.).

2.6. Visualization of in vivo release of GdDTPA from PLGA microspheres

Due to inefficient delivery of large particles into tumor tissue after intravenous administration [10], a MS-GdDTPA/SPIO/5-FU suspension (10 μL) was administered intratumorally into the MCF-7 tumor using a U-100 BD insulin syringe (28 gauge, Franklin Lakes, NJ, U.S.A.) at a dose of 550 μg per mouse, which is equivalent to 2.5 μmol/kg of GdDTPA. MRI was acquired pre- and 30 min, 2.5 hr, and 21 hr post-administration of MS-GdDTPA/SPIO/5-FU. The mouse was removed from the probe/magnet at the time of injection, and the tumor was placed back in the coil after injection. Acquisition parameters and image processing were the same as those used in the study on NS-GdDTPA/SPIO/5-FU.

2.7. Statistical analysis

Median T_1 values in the selected region-of-interest (ROI) (N=5) were compared between each time point to determine if the T_1 values in the region where the majority of nanospheres was delivered and accumulated in the tumor were significantly changed. The one-way Analysis of Variance (ANOVA) was used for omnibus F-test using StatPlus®:mac (AnalystSoft Inc., Alexandria, VA, U.S.A.) software, and the Scheffé's test was undertaken for post hoc analysis. The T_1 values were considered to be significantly different (P<0.05) when the F value is greater than the critical value of the F-distribution ($F_{\text{crit, }\alpha=0.05} = 3.89$).

3. Results

3.1. In vitro characteristics of contrast agent-loaded PLGA nano/microspheres

Scanning electron microscopy (SEM) confirmed that both carriers were spherical in shape (Fig. 2), and the sizes were approximately 194 nm for NS-GdDTPA/SPIO/5-FU and 2.6 μm for MS-GdDTPA/SPIO/5-FU (Table 1). The *in vitro* release profile of GdDTPA from NS-GdDTPA/ SPIO/5-FU was similar to that of 5-FU, indicating that GdDTPA can be used as an imaging tracer to visualize the release of 5-FU from the NS-GdDTPA/SPIO/5-FU. Both GdDTPA and 5-FU were released rapidly from NS-GdDTPA/SPIO/5-FU, *i.e.*, releases were completed within 30 min. In contrast, the release profile of GdDTPA from MS-GdDTPA/ SPIO/5-FU was significantly different from that of 5-FU, and both molecules were released slightly slower than from NS-GdDTPA/SPIO/5-FU. This result indicates that the GdDTPA used in this study is not a good surrogate for the release of 5-FU from MS-GdDTPA/SPIO/ 5-FU *in vivo*. Since a preliminary *in vitro* experiment demonstrated that the detection of the 5-FU peak in ^{19}F-MRS requires high concentration of 5-FU in the tumor site (Fig. S2), we conducted *in vivo* release monitoring only by MRI. PLGA nanospheres and microspheres were used to delineate the feasibility of the dual MR contrast technique for noninvasive monitoring of release of GdDTPA from carriers with different release profiles.

3.2. Visualization of in vivo release of GdDTPA from PLGA nanospheres

MR images of the MCF-7 xenografts acquired before and up to 2.5 hr post intravenous administration of NS-GdDTPA/SPIO/5-FU suspension are displayed in Fig. 3. Following intravenous administration of the NS-GdDTPA/SPIO/5-FU, SPIO particles generated strong T_2* contrast, which corresponds to the dark spots in the T_2* images (red arrow), indicating the region where the intact NS-GdDTPA/SPIO/5-FU were distributed in the tumor. In contrast, a T_1 reduction was observed around the areas where the NS-GdDTPA/SPIO/5-FU were localized at 30 min post-contrast, while T_1 values for the same area were restored at 2.5 hr post-contrast in the quantitative T_1 map. This indicates that GdDTPA was released from NS-GdDTPA/SPIO/5-FU soon after the intravenous administration of NS-GdDTPA/

SPIO/5-FU, and rapidly diffused away from the nanoparticles, so that T_1 enhancement became visible. As reported earlier, the estimated spatial distance between SPIO and GdDTPA to enable the detection of the T_1 effects of GdDTPA should be over 15 μm, when an echo time of 30 ms is used for breast cancer xenografts [5,11]. The position of the large dark spot remained unchanged from its initial location, indicating that the diffusion of SPIO particles was limited. It is worth noting that, in our experiments performed at a high magnetic field (9.4T) and a high concentration of SPIO particles, the T_2/T_2* effects of SPIO prevailed over possible T_1 effects. Quantitative T_1 maps give absolute T_1 values of the images on a pixel-to-pixel basis, and the concentration of GdDTPA in each pixel can be calculated using a calibration curve for a standard GdDTPA solution. Thus, quantitative T_1 maps also provide quantitative information on GdDTPA distributed in the tumor (Fig. 3a, bottom panels). A T_1 reduction was more clearly observed in the region where the majority of nanospheres was delivered and accumulated in the tumor compared to the whole tumor lobe (Fig. 3b). The regions where the release of GdDTPA occurs is clearly distinguished by the median T_1 values (Table 2). It is worth noting that the *in vivo* release observed here was consistent with the *in vitro* release profile of GdDTPA from NS-GdDTPA/SPIO/5-FU. Taken together, this *in vivo* experiment has provided conclusive evidence that the dual MR contrast technique could monitor the delivery, release, and intratumoral distribution of GdDTPA, a surrogate tracer of an anticancer agent, after intravenous administration of nanocarriers noninvasively.

3.3. Visualization of in vivo release of GdDTPA from PLGA microspheres

The release of GdDTPA from MS-GdDTPA/SPIO/5-FU delivered intratumorally is shown in Fig. 4. T_2*-weighted images identified the location of the injection site as a dark spot. T_1 maps revealed that the release of GdDTPA from MS-GdDTPA/SPIO/5-FU was predominantly observed about 30 min after the intratumoral administration of MS-GdDTPA/SPIO/5-FU. While the released GdDTPA was still detected at 2.5 hr post-administration of microspheres, no GdDTPA was detected at 21 hr post-administration. These results were also in good agreement with the *in vitro* release kinetics, which showed that the release of GdDTPA from the MS-GdDTPA/SPIO/5-FU was slower than that from the NS-GdDTPA/SPIO/5-FU, and plateaued after 4 hrs.

4. Discussion

The results presented here indicate that this technique can be used for variety of different nanocarriers, as well as for different tumor models (see Supplemental material, Fig. S3). MRI can double as a tool that can provide monitoring of the delivery, release, and distribution of cargo molecules in the target site, as well as for monitoring therapeutic progress with high-resolution anatomical and functional imaging. Therefore, MRI can be used to better understand drug delivery systems in combination with this technique, which will be conducive to more effective therapeutic strategies.

The technical issues that need to be addressed in this technique are sensitivity and the applicability of gadolinium chelates as a surrogate tracer for different drugs. MRI has inherently low sensitivity compared to radionuclide imaging or optical imaging, and MRS has even lower sensitivity. On the other hand, this unique dual-contrast mechanism enables us to distinguish between encapsulated and released molecules, and high-resolution imaging is also a significant advantage of MRI over other imaging modalities. MRI contrast agents are also well suited for longitudinal imaging, such as the monitoring of drug release for formulations or implanted devices that are intended for long-term treatment protocols. Significant efforts have been made to increase the sensitivity of MR contrast agents [12]. The conjugation of gadolinium chelates with macromolecules, such as albumin and dendrimers, helps to improve sensitivity by carrying multiple gadolinium chelates in a single

conjugate and by slowing molecular tumbling. However, since conjugation increases the molecular size of gadolinium chelates, this option is only feasible, if encapsulated drug molecules have similar molecular sizes and properties to the gadolinium chelates, and the diffusion rate/distance of the gadolinium chelates still distinct from those of the T_2/T_2* agent. Another issue is long acquisition times, but this is not a critical hurdle in clinical settings. Although it currently takes about an hour to acquire three-dimensional images with five different repetition times in order to obtain a quantitative T_1 map, quantitative T_1 maps can easily be obtained with a variable flip angle (VFA), which will make acquisition time significantly shorter [13,14]. With regard to gadolinium chelates, clinically-available gadolinium chelates are relatively small, water-soluble molecules. Although 5-FU is also a small, water-soluble molecule, the release profile of 5-FU was not similar to that of GdDTPA, as shown in Fig. 2d. Therefore, the similarity of the release and diffusion behavior between the drug and contrast agent loaded in the carriers must be confirmed prior to the *in vivo* use of this technique. It also should be noted that the possibility for the toxicity of gadolinium may increase due to an extended half-life in the body, given that gadolinium chelates are used with nanocarriers. From these standpoints, the direct detection of drug molecules by MRS is ideal because MRS does not require using a surrogate tracer, although concern remains about the sensitivity.

This technique can be applied to multiple drug carriers or implant devices by incorporating superparamagnetic iron particles into the carrier/reservoir and using gadolinium chelate as a surrogate diffusible tracer for drug molecules. Gadolinium agent must be similar to the intended drug with regard to factors such as molecular size, hydrophilicity (lipophilicity), and other physicochemical characteristics: more sophisticated comparisons between gadolinium agents and drugs may be needed in order to use them as surrogate tracers.

5. Conclusions

The intact carrier generates negative contrast enhancement due to the dominant T_2/T_2* effect of superparamagnetic iron oxide (SPIO) nanoparticles, while positive contrast enhancement is generated by GdDTPA that is released and diffused away outside the range of the T_2/T_2* effect of SPIO after the carrier has degraded. Although much work remains to be done about the use of MR contrast agents as surrogate tracers for drugs, we have here, for the first time, demonstrated the feasibility of a new MRI strategy to monitor the delivery, release, and intratumoral distribution of cargo molecules *in vivo*. This technique will also be of value for other purposes, particularly those that take advantage of the differences in the contrast mechanisms of positive and negative MRI contrast agents, which are currently under investigation.

Supplementary Material

Refer to Web version on PubMed Central for supplementary material.

Acknowledgments

We thank Ms. Nicole E. Benoit for maintaining the cell lines, Ms. Lan Wu for her technical assistance, and Ms. Mary McAllister for editing this manuscript. This work was supported by the National Institutes of Health (R21 EB008162) and The Nagai Foundation, Tokyo.

References

1. Mora L, Chumbimuni-Torres KY, Clawson C, Hernandez L, Zhang L, Wang J. Real-time electrochemical monitoring of drug release from therapeutic nanoparticles. J Control Release 2009;140:69–73. [PubMed: 19679152]

2. Port RE, Schuster C, Port CR, Bachert P. Simultaneous sustained release of fludarabine monophosphate and Gd-DTPA from an interstitial liposome depot in rats: potential for indirect monitoring of drug release by magnetic resonance imaging. Cancer Chemother Pharmacol 2006;58:607–617. [PubMed: 16506037]

3. Tung CH, Bredow S, Mahmood U, Weissleder R. Preparation of a cathepsin D sensitive near-infrared fluorescence probe for imaging. Bioconjug Chem 1999;10:892–896. [PubMed: 10502358]

4. Weissleder R, Tung CH, Mahmood U, Bogdanov AJ. *In vivo* imaging of tumors with protease-activated near-infrared fluorescent probes. Nat Biotechnol 1999;17:375–378. [PubMed: 10207887]

5. Kato Y, Artemov D. Monitoring of release of cargo from nanocarriers by MRI/MRSI: Significance of T_2/T_2* effect of iron particles. Magn Reson Med 2009;61:1059–1065. [PubMed: 19253373]

6. Walstedt RE, Walker LR. Nuclear-resonance line shapes due to magnetic impurities in metals. Phys Rev B 1974;9:4857–4867.

7. Dreher MR, Liu W, Michelich CR, Dewhirst MW, Yuan F, Chilkoti A. Tumor vascular permeability, accumulation, and penetration of macromolecular drug carriers. J Natl Cancer Inst 2006;98:335–344. [PubMed: 16507830]

8. Kato Y, Okollie B, Raman V, Vesuna F, Zhao M, Baker SD, et al. Contributing factors of temozolomide resistance in MCF-7 tumor xenograft models. Cancer Biol Ther 2007;6:891–897. [PubMed: 17582214]

9. Coe RA, Earl RA, Johnson TC, Lee JW. Determination of 5-fluorouracil in human plasma by a simple and sensitive reversed-phase HPLC method. J Pharm Biomed Anal 1996;14:1733–1741. [PubMed: 8887721]

10. Ishida O, Maruyama K, Sasaki K, Iwatsuru M. Size-dependent extravasation and interstitial localization of polyethyleneglycol liposomes in solid tumor-bearing mice. Int J Pharm 1999;190:49–56. [PubMed: 10528096]

11. Paran Y, Bendel P, Margalit R, Degani H. Water diffusion in the different microenvironments of breast cancer. NMR Biomed 2004;17:170–180. [PubMed: 15229930]

12. Raymond KN, Pierre VC. Next generation, high relaxivity gadolinium MRI agents. Bioconjug Chem 2005;16:3–8. [PubMed: 15656568]

13. Wang L, Schweitzer ME, Padua A, Regatte RR. Rapid 3D-T_1 mapping of cartilage with variable flip angle and parallel imaging at 3.0T. J Magn Reson Imaging 2008;27:154–161. [PubMed: 18050327]

14. Cheng HL, Wright GA. Rapid high-resolution T_1 mapping by variable flip angles: accurate and precise measurements in the presence of radiofrequency field inhomogeneity. Magn Reson Med 2006;55:566–574. [PubMed: 16450365]

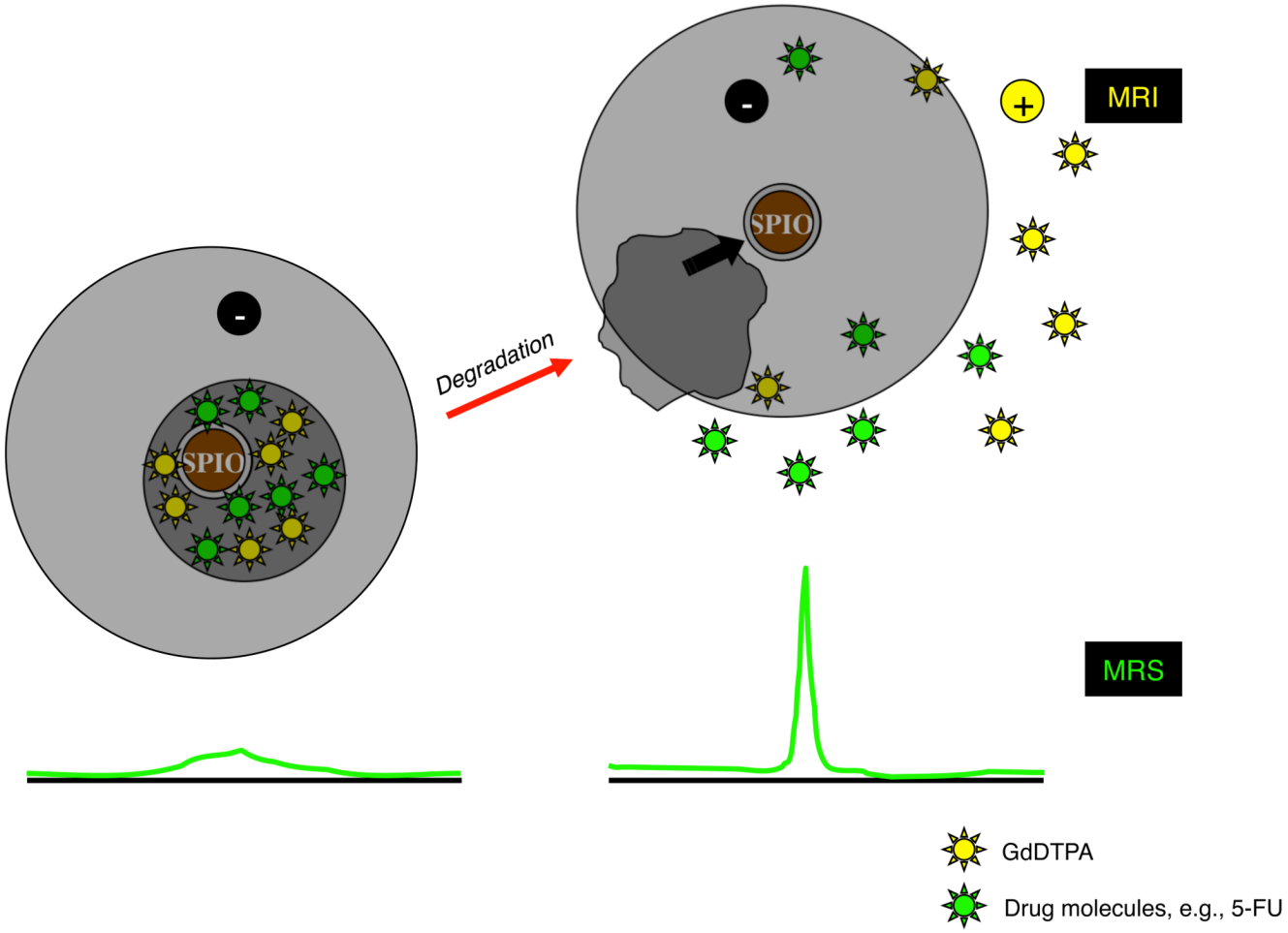

Fig. 1.

Schematic of the concept of the MR-based technique to monitor the release of cargo molecules by MRI/MRS. Intact GdDTPA/SPIO-loaded carriers generate strong negative contrast enhancement in MRI due to the prevailing T_2/T_2* effects of SPIO (left panel). For MRS, SPIO-loaded intact carriers broaden the resonance line of drug molecules; for example, anticancer agents, such as 5-FU, due to the *T2** effects of SPIO (left panel). Upon release, the free GdDTPA generates positive contrast enhancement in areas beyond the *T2*/*T2** effects of SPIO that has limited diffusion range, and the free drug molecules demonstrate a narrow resonance line (right panel). Therefore, we can (i) identify the location where carriers are delivered as a dark spot on MRI; (ii) detect a release of GdDTPA by a decrease in T_1 values, which is caused only by the "released" GdDTPA in MRI, and detect a release of cargo drugs by the appearance of a narrow resonance line of the "released" drug molecules in MRS; and (iii) see the distribution of the "released" GdDTPA by a decrease in the *T1* values in quantitative *T1* maps. The concept of this technique was proven by *in vitro* phantom studies in our previous report [5].

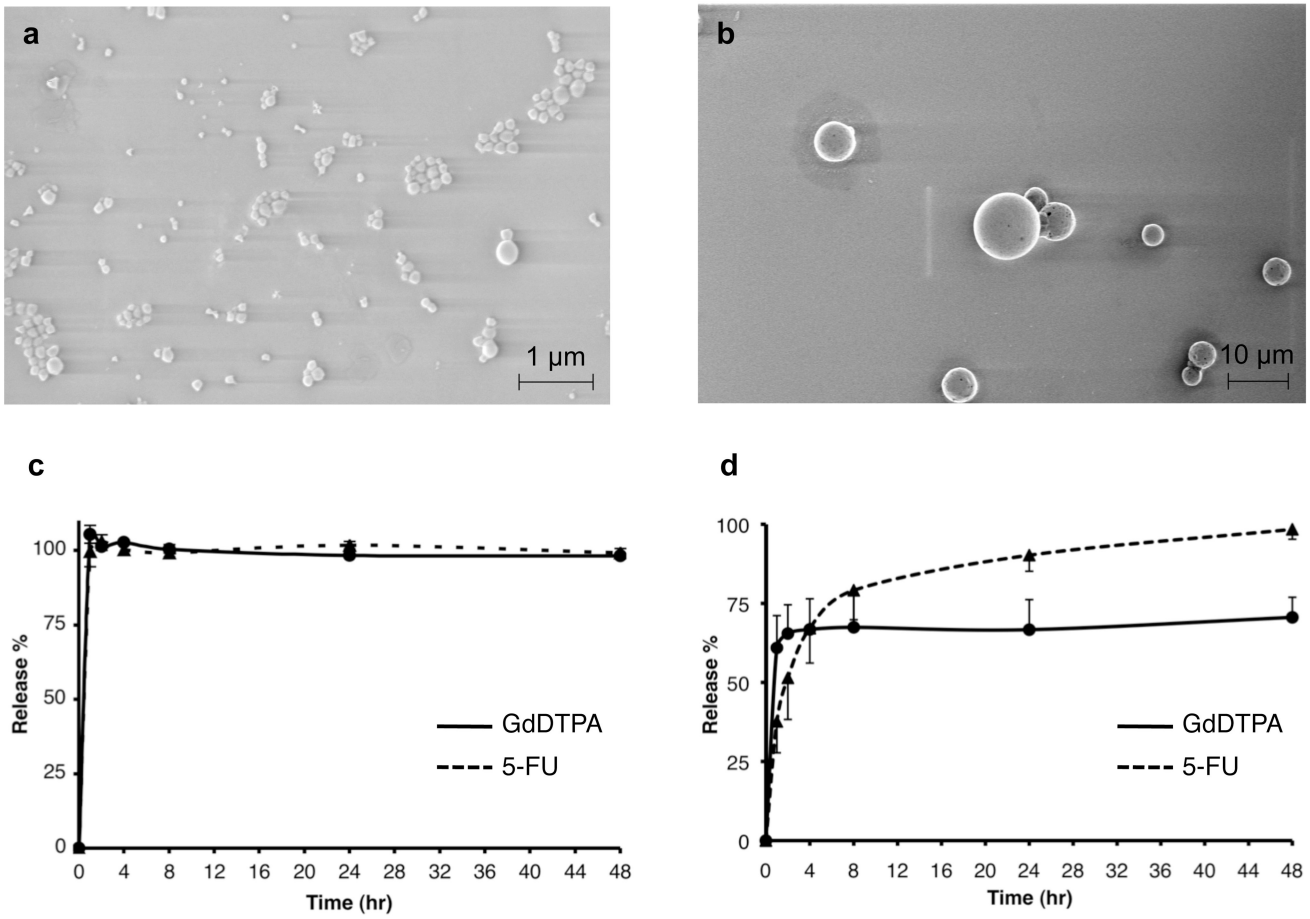

Fig. 2.

In vitro characteristics of PLGA nano/microspheres. Scanning electron microscope (SEM) images of **(a)** PLGA nanospheres (NS-GdDTPA/SPIO/5-FU) and **(b)** PLGA microspheres (MS-GdDTPA/SPIO/5-FU). *In vitro* release profiles of GdDTPA and 5-FU from **(c)** NS-GdDTPA/SPIO/5-FU and **(d)** MS-GdDTPA/SPIO/5-FU. The quantification of GdDTPA was performed by T_1 measurement of release medium with a calibration curve using standard Omniscan®, based on the linear relationship between GdDTPA concentration and $1/T_1$ (R^2=0.999 for 0.5 μM – 50 mM on 9.4T MRI). The quantification of 5-FU was performed using reverse-phase HPLC. Please see supplemental materials for details.

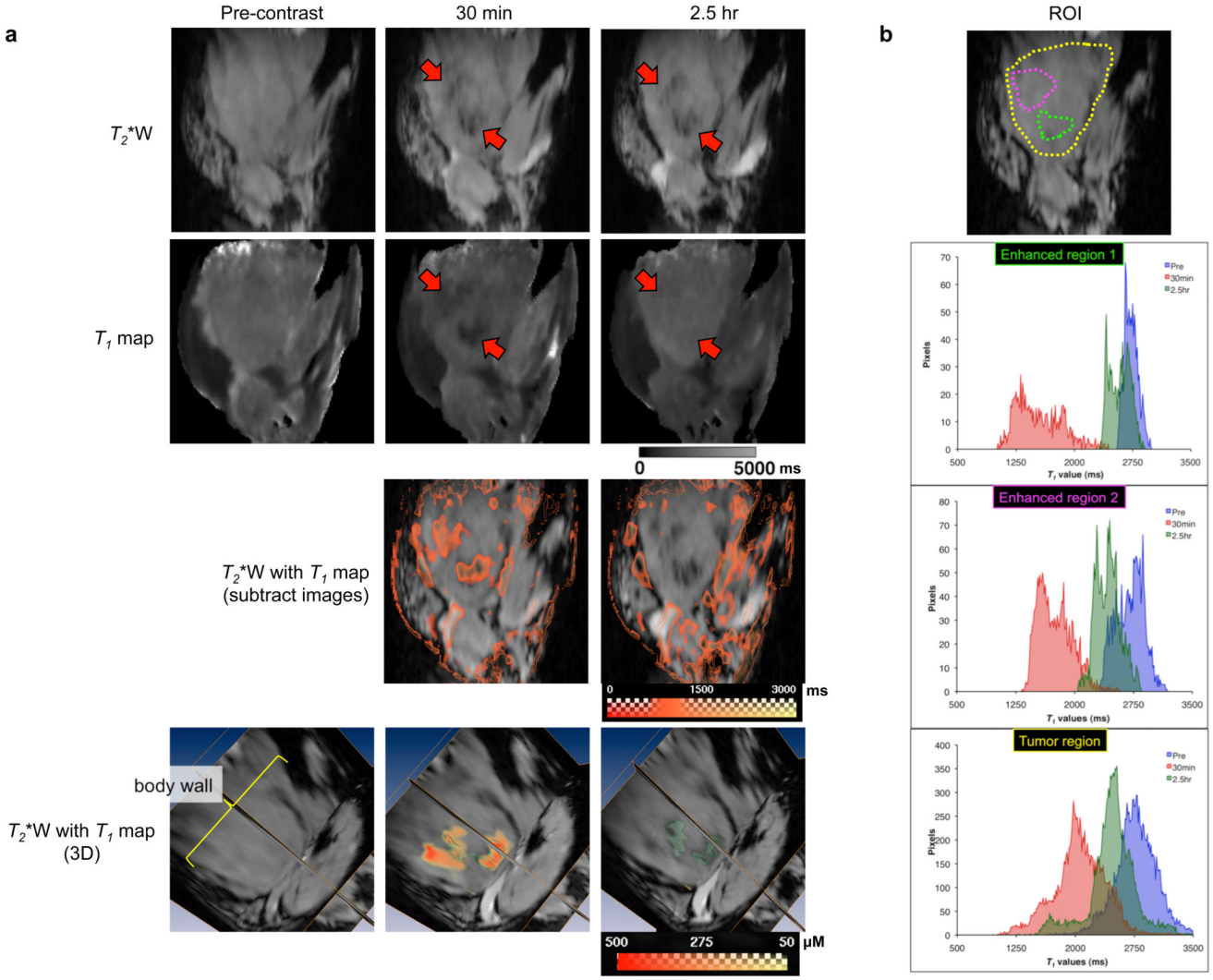

Fig. 3.

Visualization of the *in vivo* release of GdDTPA from NS-GdDTPA/SPIO/5-FU by the dual MR contrast technique. **(a)** MR images of the representative tumor over time. T_2*-weighted images (top panels) and T_1 maps (second row of panels) were from 10 stacked slices (≈1.25 mm) out of 128 slices. From the top panels, we could identify the location of NS-GdDTPA/SPIO/5-FU as a dark spot (a red arrow) on T_2*-weighted MRI. We could observe a decrease in T_1 values in the tumor around the area where the NS-GdDTPA/SPIO/5-FU were delivered (a red arrow) on the T_1 map only 30 min after administration (second row of panels). The panels in the third row represent the subtraction images of the T_1 map (pre-contrast minus post-contrast) overlaid on T_2*-weighted images. We could clearly see the changes in T_1 values around the area where the nanospheres were located. In the bottom panels (T_2*-weighted images overlaid with quantitative T_1 values), the green channel represents SPIO-loaded PLGA nanospheres, and the red-yellow channel indicates the distribution of GdDTPA released from the NS-GdDTPA/SPIO/5-FU in the tumor. We were able to determine the spatial distribution of GdDTPA released from the NS-GdDTPA/SPIO/5-FU quantitatively. Scale bars represent the range of T_1s in milliseconds for the panels of the middle two rows, and the range of the concentration of GdDTPA in micromolar is depicted in the bottom row panels. **(b)** Selection of a region-of-interest (ROI) in the tumor, and

histograms of the T_1 values of the selected ROI. T_1 values were calculated within selected ROIs encircled in the yellow (the whole tumor lobe), green (the area where the NS-GdDTPA/SPIO/5-FU were distributed), and pink (the area where the NS-GdDTPA/SPIO/5-FU were distributed) regions. The blue, red, and green channels represent pre-, 30 min, and 2.5 hr-post i.v. administration of the NS-GdDTPA/SPIO/5-FU, respectively. From the histograms, we could clearly distinguish whether nanospheres remained intact or released GdDTPA, especially around the area where nanospheres were delivered (also see Table 2).

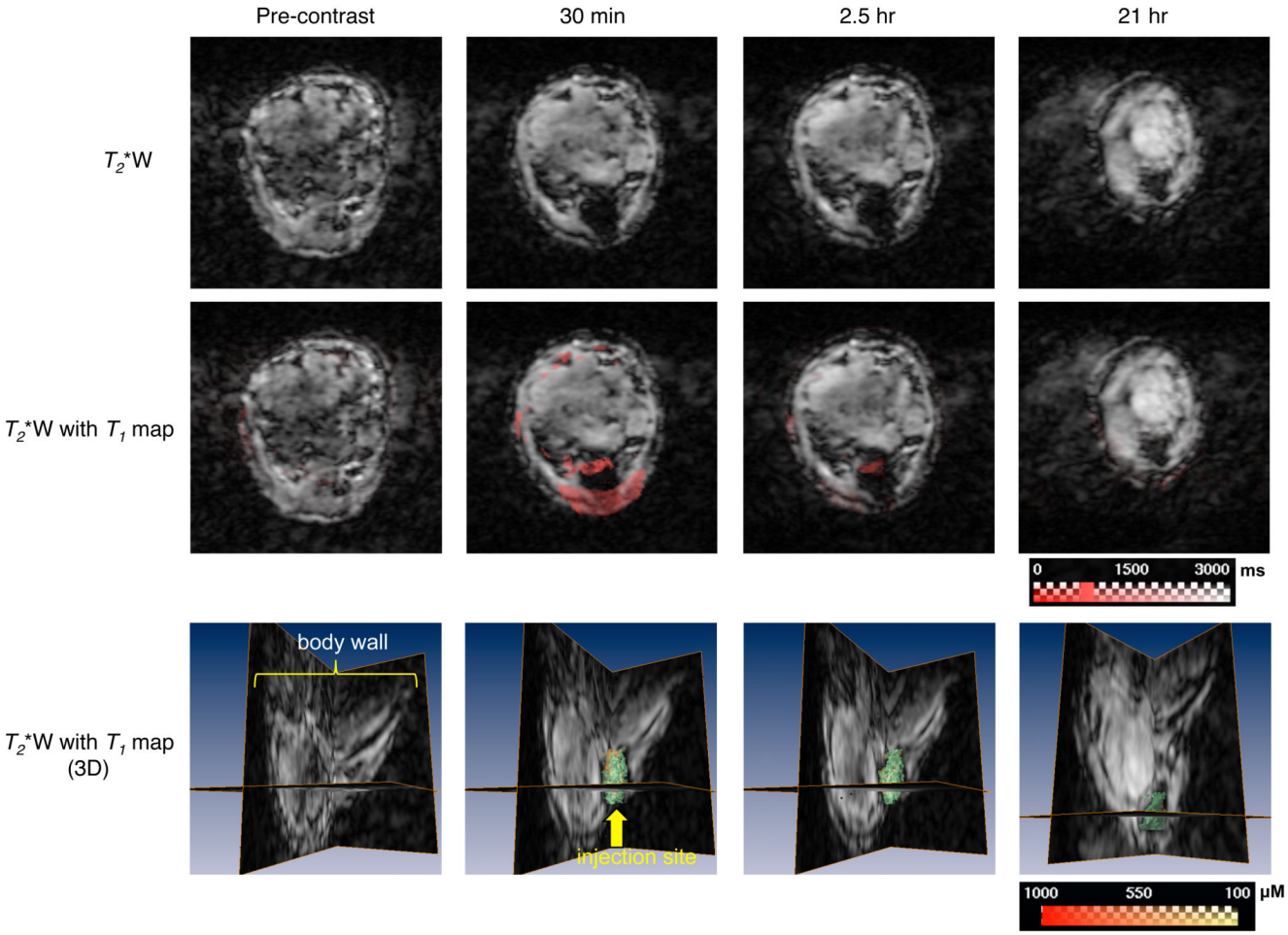

Fig. 4.

In vivo monitoring of the release of GdDTPA from MS-GdDTPA/SPIO/5-FU by dual MR contrast technique in MCF-7 breast cancer xenografts. Two-dimensional MR images were from one representative slice out of 128 slices in the z-direction. From the top row panels, we could identify the location of MS-GdDTPA/SPIO/5-FU as a dark spot on T_2*-weighted MRI. We could observe, on the T_1 map, a decrease in the T_1 values of the tumor around the area where the PLGA microspheres were injected, notably at 30 min, and slightly, at 2.5 hr after intratumoral administration (panels of the middle row). In the bottom panels (T_2*-weighted images overlaid with quantitative T_1 values), the green channel represents SPIO-loaded PLGA microspheres, and the red-yellow channel indicates the distribution of GdDTPA released from the MS-GdDTPA/SPIO/5-FU in the tumor. Similar to the intravenous injection of NS-GdDTPA/SPIO/5-FU, we were able to determine the spatial distribution of GdDTPA released from the MS-GdDTPA/SPIO/5-FU quantitatively. Scale bars represent the range of T_1s in milliseconds in the panels of the middle row, and the range of the concentration of GdDTPA in micromolars in the bottom row.

Table 1

In vitro characteristics of PLGA nano/microspheres

	Diameter (nm)[1, 2]	Polydispersity Index ± S.D.	ζ-potential (mV) ± ζ deviation[1]	GdDTPA contents (nmol/mg NPs) ± S.D.	5-FU contents (nmol/mg NPs) ± S.D.
NS-GdDTPA/SPIO/5-FU	194 ± 10	0.095 ± 0.042	−2.2 ± 0.5	12.8 ± 2.7	4.3 ± 0.7
MS-GdDTPA/SPIO/5-FU	2612 ± 1137	0.801 ± 0.273	−7.0 ± 1.6	90.6 ± 18.4	7.0 ± 1.7

[1] Nanoparticles were dispersed in PBS (pH 7.4) for the size measurement, and dispersed in 10 mM of NaCl for the ζ-potential measurement.

[2] The hydrodynamic diameter of nanoparticles was calculated by the Stokes-Einstein equation.

Table 2

Changes in T_1 values of region-of-interests (ROIs) where T_1 reduction was observed in the tumor over time

	median T_1 value (ms) ± S.E.	Statistical differences ($F_{crit, \alpha=0.05} = 3.89$)[1]		
		Pre *vs.* 30 min	**30 min *vs.* 2.5 hr**	**2.5 hr *vs.* Pre**
Pre-injection	2826 ± 88	$F = 68.55$ SS	—	
30 min post-injection	1715 ± 53		$F = 40.55$ SS	—
2.5 hr post-injection	2570 ± 55	—		$F = 3.65$ NS

[1] T_1 values of the enhanced regions in the tumor were significantly dropped at 30 min post-injection of NS-GdDTPA/ SPIO/5-FU, and T_1 values were restored to pre-injection values at 2.5 hr after injection. SS: Statistically significant ($P<0.05$); NS: Not significant.